Strength analysis of membrane structures for the support of future solar Islands

Master Thesis in Marine Technology - 2023

Mehmet Doğancan Ecemiş, Svein Sævik and Virgile Delhaye

NTNU Norwegian University of Science and Technology

SFI BLUES

Introduction

The objective of this study is to provide a comprehensive analysis of membrane materials, their mechanical behavior, and their applications in various industries. Membranes have gained significant attention due to their lightweight nature and customizable selectivity, making them an ideal solution for achieving sustainable operations. Understanding the mechanical properties and structural behavior of membranes is crucial for optimizing their performance and ensuring their reliable application in diverse fields.

Objective and Scope

A combined approach of computational modeling and experimental testing was employed to investigate the mechanical behavior of membrane materials. A computational model was developed using ABAQUS software, incorporating material properties, geometrical parameters, and loading conditions. Experimental tests were conducted at the SINTEF Material Laboratory, subjecting membrane specimens to various loading conditions.

The computational model was validated by comparing simulation results with experimental data from uniaxial tensile tests and dynamic mechanical analysis experiments. Uniaxial tensile tests provided insights into the material's response to uniaxial loading, while dynamic mechanical analysis examined its behavior under cyclic loading and varying stress rates within a specific frequency range.

The computational model was calibrated and adjusted based on the experimental data to accurately capture the mechanical response of the membrane materials.

Experiment

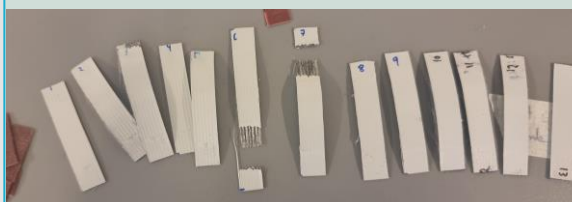Figure 1 All the tensile specimens after runs (L:150 mm W: 30mm)

Figure 2 All the DMA specimens after runs (L:30 mm W: 10 mm)

Tensile tests measure the response of a membrane material to uniaxial loading using a universal testing machine, providing information on its mechanical properties such as strength, elasticity, and elongation.

DMA tests, performed using the Gabo Explorer 150N machine, examine the material's behavior under cyclic loading and varying stress rates within a specific frequency range (0.01-50 Hz), offering insights into its viscoelastic properties and response to dynamic forces. Figures on the left display post-experiment specimens.

Modelling and Calibration

In the tensile test, a total of 14 specimens were used, and the experimental data was obtained using Ecorr DIC software. In the DMA test, a total of 9 specimens were used and the DMA software of the test machine gave the results. Figure 3 compares material property determination in experiments and ABAQUS software, with the use of DIC software's virtual extensometer. Same points are selected on specimen and model for accurate alignment and consistent results. Two models were employed: Elasto-plastic and hyperfoam with added viscoelasticity. Elasto-plastic model required calibration of yield stress and plastic strain values to achieve a close match with experimental stress-strain curves in Figure 4 with $\sigma_{calibrated}$ equation.
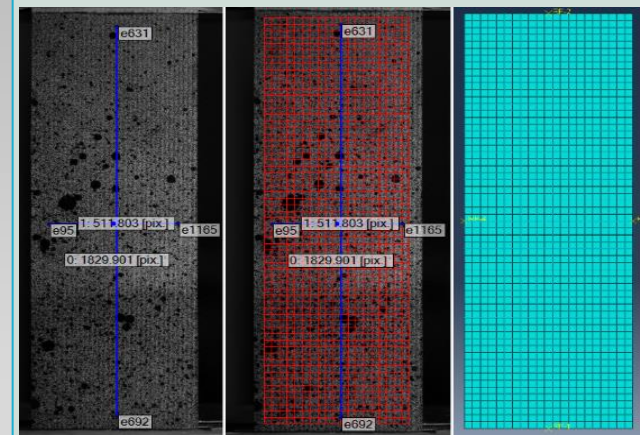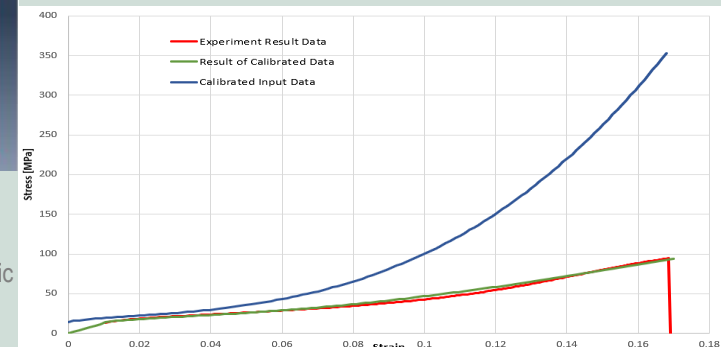

Figure 3 Virtual extensometer on DIC and RPs on the model

The hyperfoam model utilizes Prony coefficients with $G_R(f)$ equation to describe the viscoelastic behavior of materials, representing their relaxation. Prony coefficient calibration involves adjusting the values to match experimental data, ensuring an accurate representation of the material's viscoelastic response. Figure 5 displays the extended frequency specimens, showing a good fit between the Prony data and experimental data for each specimens. The frequency range is consistent across all specimens, while the static stress values differ (10 MPa for S1L, 40 MPa for S8L, and 50 MPa for S11L).

Figure 4 Elasto-plastic model calibration on stress strain values

$$\sigma_{calibrated} = (\sigma_{abaqus}) + (C \cdot (\varepsilon_{new} - \varepsilon_{first})^3)$$
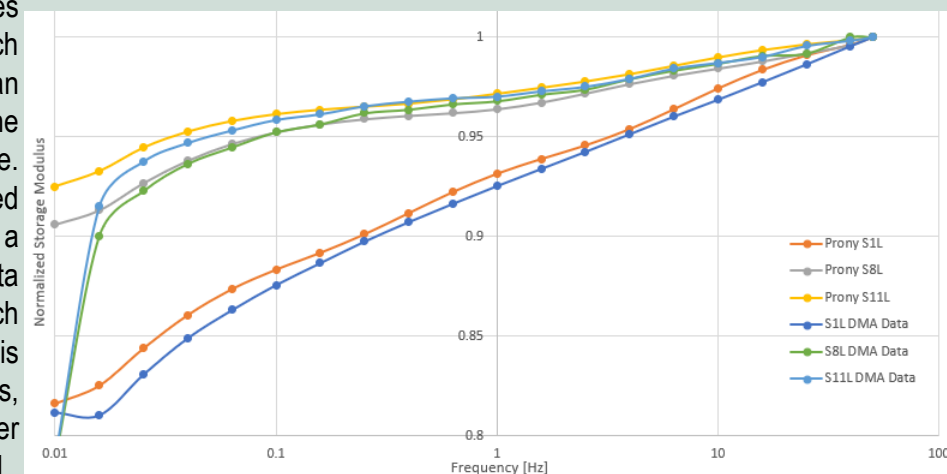

Figure 5 Extended DMA specimens and prony obtained data comparison

$$G_R(f) = G_0 \left(1 - \bar{g}_1{}^P (1 - e^{-t/\tau_1^f}) - \bar{g}_2{}^P (1 - e^{-t/\tau_2^f}) - \bar{g}_3{}^P (1 - e^{-t/\tau_3^f}) \right)$$
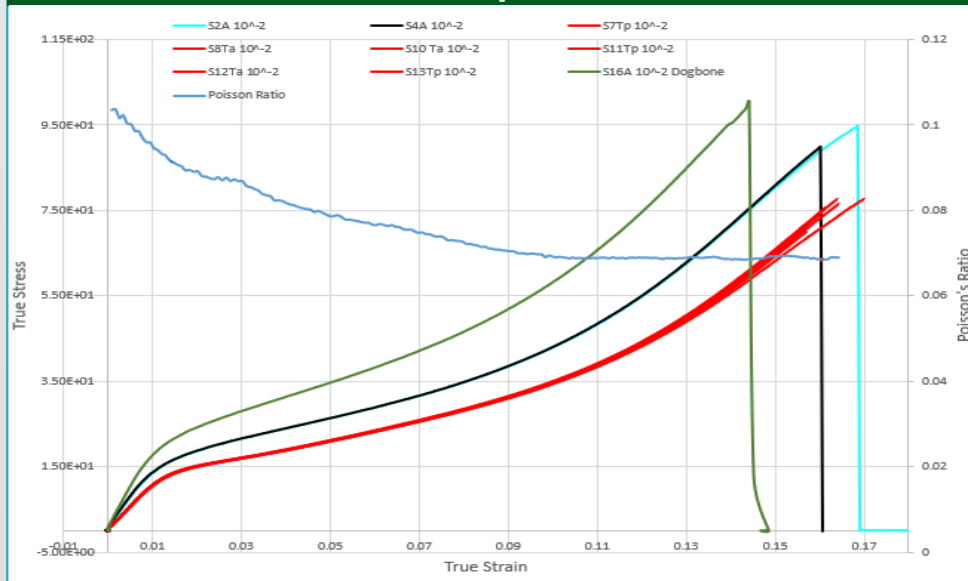
Experimental Results

Figure 5 Stress-Strain for Axial and Transversal Specimens at 1E-2 Strain with Poisson's Ratio

Figure 5 illustrates the results for all the specimens tested at a strain rate of 1E-2, as it provided the most satisfactory outcomes compared to the 1E-1 and 10E-3 strain rates, with the Poisson's ratio. The most representative curve shows in cyan color S2A 1E-2 specimen, was selected for the simulation.
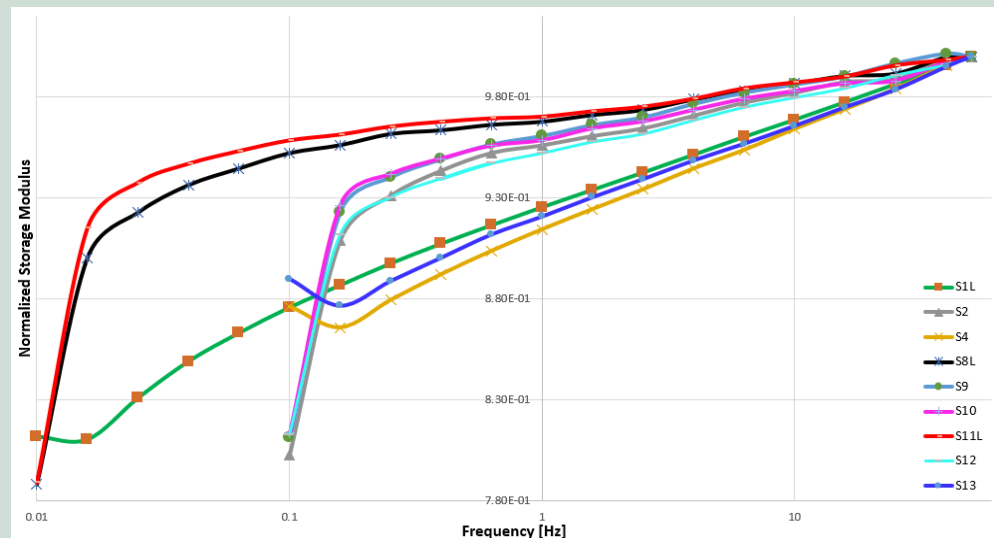

Figure 6 All the DMA specimens results in logaritmic scale

Figure 6 is provided to enhance the visibility of the curves by using a logarithmic scale. The normalized storage modulus is calculated by dividing each storage modulus value by the highest storage modulus value obtained from the corresponding specimen. This normalization technique enables a more accurate evaluation of the relative differences in storage modulus across the various specimens. By applying data normalization, a comprehensive understanding of the relative variations in storage modulus among the analyzed specimens can be obtained.

Simulation and Experimental Results Comparison

Figure 7 clearly illustrates the resemblance between the strain distribution values obtained from both the model and the specimen on the DIC software. Notwithstanding minor disparities, the figures depict a close alignment of values, particularly in the vicinity of the 0.20 strain region. This similarity is indicative of the consistent behavior observed just before the fractures. Figure 8 shows the experiment and elasto-plastic simulation results comparison.
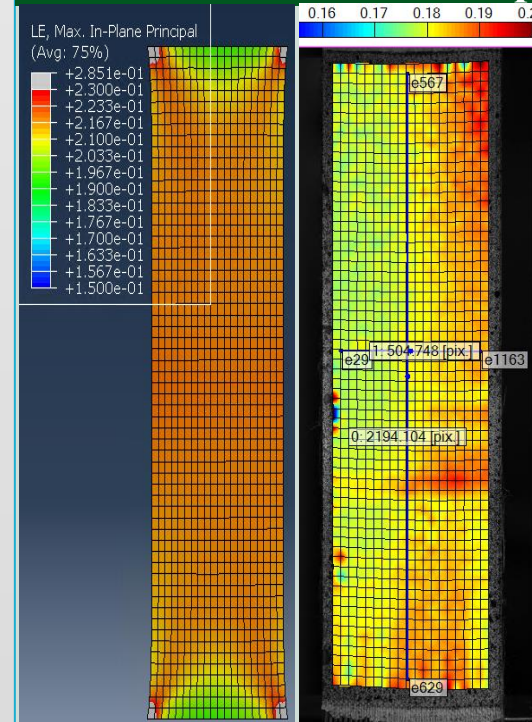

Figure 7 Comparing Strain Distributions: Model vs. Specimen.

Figure 8 . Simulation vs Experiment Result

The hyperfoam model analysis was conducted using load-driven and displacement-driven models, and the results were compared with experimental data. Figure 9 illustrates the comparison of storage modulus curves, showing a good fit between the simulated and experimental results. To ensure accurate comparisons, a total of six simulations were performed at different frequency rates: 0.01, 0.1, 1, 10, 50, and 100 Hz. These frequency values were chosen to align with the frequencies used in the experimental setup.
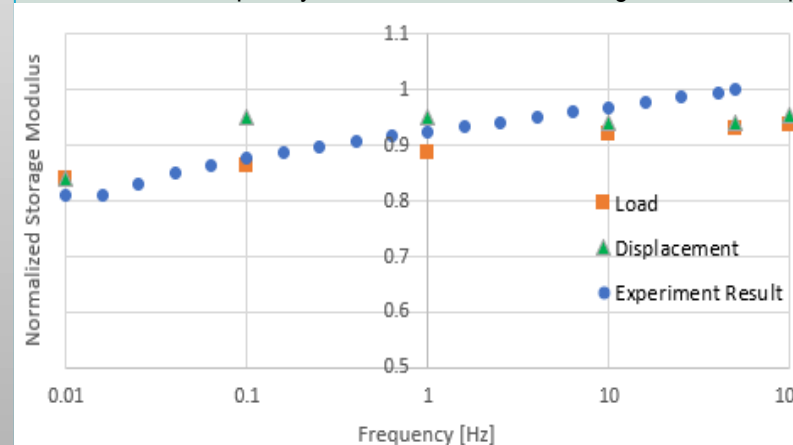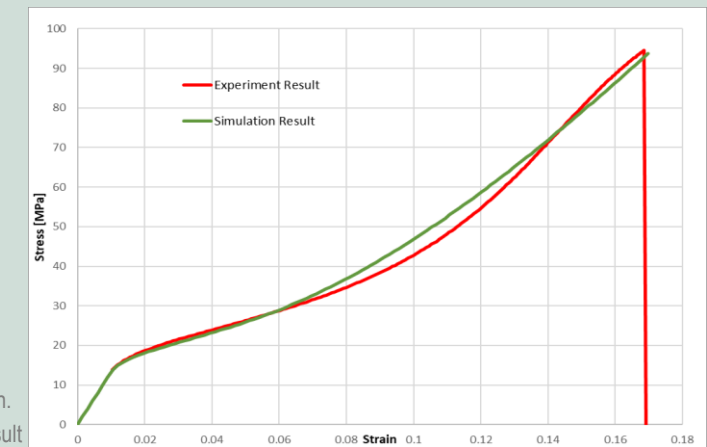
By using the same frequency values, it was possible to assess the behavior of the material at the exact same points as in the experiments, facilitating meaningful comparisons. The close agreement between the simulation results and experimental data demonstrates the capability of the models to accurately capture the viscoelastic behavior of the material under different frequency conditions.

Figure 9 . DMA Experiment Results with Load-driven and Displacement-driven Models

Conclusion

In conclusion, the results of both simulations and experiments demonstrate a satisfactory fit on the graphs, allowing for meaningful comparisons in the Master's thesis. While the simulated DMA experiments and tensile tests do not precisely replicate real-world conditions, they closely approximate them. However, limitations exist within the current version of ABAQUS software in fully describing material behavior and criteria. The hyperelastic model lacks the ability to predict failure or isotropy, while the elasto-plastic model cannot incorporate viscoelasticity. To address these limitations, two different simulation models were utilized in the thesis. The elasto-plastic model was suitable for assessing excessive loads and ultimate limit state scenarios, whereas the hyperelastic-viscoelastic model was recommended for small cyclic or deadweight loads. Unfortunately, due to time constraints, it was not possible to utilize a UMAT code to modify the ABAQUS models for comprehensive analysis. Furthermore, the Young's Modulus values were slightly lower than reality due to the fitting of the hyperelastic model, but using the hyperfoam model yielded better results at small strains. To improve curve fitting, additional points were added at the beginning of the curve during optimization. In summary, despite certain limitations, the study's findings contribute valuable insights into membrane behavior and support the development of more accurate computational models for future analyses.

Key References

[1] . Knippers, J. Cremers, M. Gabler, and J. Lienhard, Construction manual for polymers+ membranes: materials, semi-finished products, form finding, design. Walter de Gruyter, 2012

[2] M. Seidel, Tensile surface structures: a practical guide to cable and membrane construction. John Wiley & Sons, 2009.

[3] . L. Marbaniang, S. Dutta, and S. Ghosh, "Tensile membrane structures: An overview," Advances in Structural Engineering, pp. 29–40, 2020

[4] C. G. Huntington, Tensile fabric structures: design, analysis, and construction. American Society of Civil Engineers, 2013

[5] M. A. Tapia-Romero, M. Dehonor-Gómez, and L. E. Lugo-Uribe, "Prony series calculation for viscoelastic behavior modeling of structural adhesives from dma data," Ingeniería, investigación y tecnología, vol. 21, no. 2, 2020